IEEE Access
Multidisciplinary | Rapid Review | Open Access Journal

Received April 29, 2019, accepted May 20, 2019, date of publication May 30, 2019, date of current version June 18, 2019.

Digital Object Identifier 10.1109/ACCESS.2019.2920095

MEMS 3D DR/GPS Integrated System for Land Vehicle Application Robust to GPS Outages

WOO JUNG PARK[1], JIN WOO SONG[2], (Member, IEEE), CHANG HO KANG[3], JAE HONG LEE[1], MYUNG HWAN SEO[4], SANG YEON PARK[4], JONG YUN YEO[4], AND CHAN GOOK PARK[1], (Member, IEEE)

[1]Department of Mechanical and Aerospace Engineering / Automation and System Research Institute, Seoul National University, Seoul 08826, South Korea
[2]School of Intelligent Mechatronics Engineering, Sejong University, Seoul 05006, South Korea
[3]College of Engineering, Research Institute of Engineering and Technology, Korea University, Seoul 02841, South Korea
[4]IVS(In-Vehicle Solution) Development Team, Hyundai MNSOFT, Seoul 04365, South Korea

Corresponding author: Chan Gook Park (chanpark@snu.ac.kr)

This work was supported in part by the Hyundai MNSOFT, Inc.

ABSTRACT In this paper, we propose a MEMS 3D DR/GPS integrated system which provides 3D attitude and position information for land vehicle application. Since low-cost MEMS-IMU provides data with large bias, it is hard to obtain an accurate position of the land vehicle, especially during GPS outages. To improve the performance of the MEMS-based navigation system, odometer-based 3D DR/GPS formulation is proposed. The proposed algorithm uses 1D speed information for obtaining 3D position and extended Kalman filter (EKF) to compensate for navigation errors. An error model for the EKF is developed, including the odometer scale factor, which may change over various environments and require an accurate value. By substituting a MEMS INS/GPS system to 3D DR/GPS system, the velocity and position errors of navigation solution are reduced. Since the proposed system estimates 3D attitude and position unlike conventional DR/GPS system, it suppresses navigation errors effectively when a land vehicle goes uphill and downhill even for the GPS outages. Besides, the adaptation rule for measurement noise covariance is applied to improve navigation performance. The proposed method is tested for a land vehicle in an urban area, including GPS outages. The experimental results show that the proposed MEMS 3D DR/GPS system provides a more stable navigation solution with fewer position errors.

INDEX TERMS MEMS DR/GPS integrated system, 3D dead reckoning, noise covariance adaptation.

I. INTRODUCTION

Inertial navigation system (INS) provides a vehicle's position, velocity, and attitude information in a high sampling rate without external disturbance [1]–[3]. However, the accuracy of the INS depends on the specification of the inertial sensors, and the navigation errors diverge as time goes on [3]. The global positioning system (GPS) provides position information with sufficient long-term reliable accuracy [4]. On the other hand, GPS is vulnerable to external disturbance such as jamming and difficult to obtain a reliable solution in a tunnel or GPS multipath area [4], [5]. To overcome both weaknesses, INS/GPS integrated system is widely used [1]–[7].

INS/GPS integration technique is widely used not only for aerial vehicles but also for land vehicles [8], [9]. It also becomes one of the fundamental navigation systems for autonomous land vehicles because it can provide high rate navigation solutions without being affected by the external environment. For the autonomous navigation, an accurate navigation solution, which can provide a stable solution for more than 5 minutes during GPS outages such as underground parking lot or tunnel, is necessary because autonomous land vehicles require seamless navigation.

Recently, microelectromechanical system (MEMS) technology has become commercially available and MEMS-based INS/GPS systems are researched by many groups [4], [10]–[16]. In GPS outages, the navigation errors of MEMS-based INS/GPS system diverge rapidly due to low performance of sensors. To solve this problem, additional sensors such as odometer and magnetometer are used to correct the navigation errors. Previous works [4], [11] combined odometer to correct velocity error and barometer to correct altitude error, but the performance of the corrected system was not sufficient for 3D applications.

The associate editor coordinating the review of this manuscript and approving it for publication was Sanket Goel.

To improve inertial navigation performance, Rauch-Tung-Striebel (RTS) smoother and nonholonomic constraints (NHC) were used to bound position and velocity error in GPS outages [10]. However, RTS smoother is not appropriate in real-time applications since it requires post-processing. Similarly, NHC and magnetometers were used to increase heading accuracy [11]. NHC is the kinematic constraint of a land vehicle that assumes the speed perpendicular to the forward direction of the vehicle is zero. It improves the navigation performance of the vehicle only when the forward speed and the vehicle's attitude are accurate and there is no side-slip. Magnetometers were calibrated to provide heading measurement to navigation system in [14]–[16], but using magnetometers in the vehicle is inappropriate because they are prone to be contaminated by the magnetic disturbances. Previous works [17], [18] proposed integrating landmark based vision system to INS system, which has benefits in weight, cost, and power consumption. Since GPS quality is not guaranteed for all area, map matching algorithm using adaptive fuzzy network was proposed [19]. Also, Urban Trench algorithm considering Non-Line-Of-Sight (NLOS) satellites was developed using map information [20]. However, they need a precise map or other infrastructures for all regions where the vehicle goes.

In addition to the INS/GPS integration, modified fault detection and isolation (FDI) algorithm was proposed to select and use GPS data with high accuracy [21], which focused more on GPS signals and short term outages, and did not consider navigation performance in wide GPS outage area. Previous work [22] proposed a land vehicle system based on MEMS-IMU that combined with sliding-mode observer (SMO) which made virtual sensor data. While the performance was evaluated at GPS outage area for 60 seconds to 80 seconds, the INS performance for a long time GPS outage was not guaranteed, which should be verified for 3D land vehicle applications and autonomous navigation.

Because these researches basically use INS algorithm which calculates velocity by integrating acceleration from MEMS accelerometers with large bias, it causes large navigation error. For example, an accelerometer in MEMS IMU (SMI 130, Bosch) has 70mg bias. Even though 90% of accelerometer bias is compensated, $1/2 \times 7mg \times (10s)^2 = 3.5m$ of position error is occurred in GPS outage for 10 seconds.

To reduce navigation error caused by MEMS grade IMU, dead reckoning (DR)/GPS integration which uses odometer and gyros for calculating position is also studied [23]–[33]. The main difference between the DR/GPS and INS/GPS is how to obtain velocity. Since DR/GPS uses velocity obtained by odometer directly, the velocity error is lower than that for the INS case which integrates acceleration from MEMS accelerometers with a large bias to obtain velocity. Because velocity error induces attitude error by NHC, and it also increases position error by integration, the velocity error should be reduced essentially for accurate navigation solution. Fig. 1 shows an example for the comparison of conventional DR/GPS and MEMS-based INS/GPS system combined with the odometer at GPS outage area. The vehicle is going down along the circular trajectory. As MEMS accelerometer bias has not been compensated fully for a long time, the velocity error becomes larger and the estimated circular trajectory begins to be distorted.

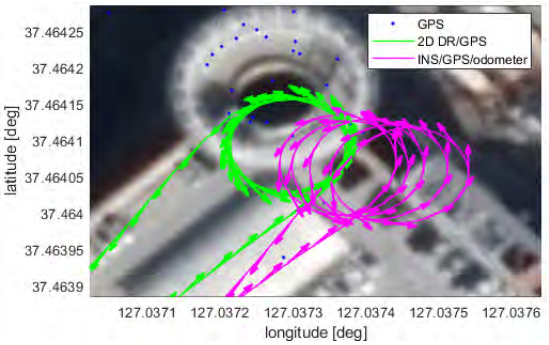

FIGURE 1. Performance degradataion of conventional INS/GPS system at GPS outage area.

Previous works [29], [30] proposed methods to estimate vehicle's attitude accurately by compensating external accelerations of the vehicle. Performance analysis was done at GPS outage areas according to combination of sensors including wheel speed sensor, steering angle sensor, and yaw rate sensor [31]. To improve navigation performance with additional sensors, visual odometry-based algorithms were also studied [32], [33]. But most of these researches focus on 2-dimensional position, velocity, and acceleration, which can increase navigation error at uphill and downhill in land vehicle applications since they do not consider pitch attitude. Especially when a vehicle moves down to the underground parking lot and goes back to the road, the 2D solution presents significant position error, which must be avoided for autonomous navigation. Reduced inertial navigation system (RISS), a 2D navigation algorithm using one single-axis gyroscope and two-axis accelerometers with odometer, was researched in [34]. In [35]–[37], RISS is developed to 3D RISS by considering roll, pitch, and yaw angles. However, 3D RISS does not estimates the odometer scale factor, which can vary over time or circumstances.

Since slight odometer scale factor error can induce large navigation error, it is important to accurately estimate it. Previous works [3], [38]–[40] estimated the odometer scale factor in INS/GPS/odometer system which will be described in section II-A. However, these researches related to INS/GPS/odometer are also based on INS/GPS, which uses acceleration integration for obtaining velocity, so that it causes larger velocity and position error than DR/GPS which uses velocity information directly without integration. Self-calibration and in-motion alignment process were proposed in [41]–[43] to estimate both misalignment and odometer scale factor. These approaches do not use attitude measurement, so their navigation performance are limited.

Also, performance improvement will not be consistent in various scenarios, especially in scenarios with dynamic motion. In [44], odometer scale factor was estimated using high-precision carrier-phase differential GPS (CDGPS) and calibrated with tire temperature. In [45], odometer was substituted to frequency modulated continuous wave (FMCW) radar which can measure the vehicle's velocity more accurately, and showed that it improves the navigation performance significantly. But high-precision CDGPS and FMCW radar are not low-cost navigation system.

To address all these issues, MEMS-based 3-dimensional DR/GPS system is proposed in this research. Since DR/GPS system is expanded from 2D to 3D, z-axis position, attitude, and 3-axis gyro bias are estimated additionally. Also, to reduce overlapped state variables, velocity and acceleration are not estimated but odometer scale factor is estimated instead and it enables estimating odometer speed, which implies no odometer settings are required. Therefore, the proposed algorithm can be applied to all automotive navigation systems installed in various models with different odometer scale factors. To sum up, 10 state variables of the proposed system are position, odometer scale factor, attitude, and gyro bias. To improve attitude accuracy, g-slave mode attitude calculated from acceleration is used as measurements, so that small attitude and position errors can be sustained during GPS outage. By integrating GPS and barometer, the altitude accuracy can be improved as well. Performance of the proposed system was verified through comparison in vehicle test with MEMS INS/GPS method combined with odometer, which consists of extended Kalman filter, and a conventional 2D DR/GPS method.

This paper is organized as follows. In section II, the conventional navigation algorithms are explained. In section III, the proposed MEMS 3D DR/GPS system is described. The experimental test results are presented in section IV, and the conclusion is presented in section V.

II. CONVENTIONAL NAVIGATION ALGORITHMS

In the MEMS-based navigation, INS/GPS/odometer system and 2D DR/GPS system are the most widely used systems. These systems are explained briefly in the following section A and B.

A. INS/GPS/ODOMETER SYSTEM

In pure navigation process of INS/GPS system, the position, velocity, and attitude update are done as (1-3) [1], [3].

$$\dot{\mathbf{p}} = \begin{bmatrix} \dot{L} & \dot{l} & \dot{h} \end{bmatrix}^T = \begin{bmatrix} \frac{v_N}{R_m+h} & \frac{v_E}{(R_t+h)\cos L} & -v_D \end{bmatrix}^T, \quad (1)$$

$$\dot{\mathbf{v}} = \begin{bmatrix} \dot{v}_N & \dot{v}_E & \dot{v}_D \end{bmatrix}^T = \mathbf{C}_b^n \mathbf{f}^b - (2\boldsymbol{\omega}_{ie}^n + \boldsymbol{\omega}_{en}^n) \times \mathbf{v} + \mathbf{g}^n, \quad (2)$$

$$\dot{\mathbf{q}} = \frac{1}{2}\mathbf{q}^*(\boldsymbol{\omega}_{ib}^b - \mathbf{C}_n^b(\boldsymbol{\omega}_{ie}^n + \boldsymbol{\omega}_{en}^n)), \quad (3)$$

where $\mathbf{p}$, $\mathbf{v}$, $\mathbf{q}$ are the position, velocity, and attitude in quaternion, L, l, h are the position in latitude, longitude, height, and subscript N, E, D represent the north, east, and vertical down direction in the navigation frame, respectively. $\mathbf{C}_b^n$ is a direction cosine matrix from body frame to navigation frame, and $\mathbf{g}^n$ is a gravity. Gravity is calculated using WGS84 earth ellipsoidal model. $\mathbf{f}^b$, $\boldsymbol{\omega}_{ib}^b$ are acceleration and angular rate measured from body frame, respectively. Symbol $\cdot$ represents the time derivative of the variable, and * means the quaternion multiplication. $\boldsymbol{\omega}_{ie}^n$, $\boldsymbol{\omega}_{en}^n$ are earth rate and transport rate measured from navigation frame, respectively. Using the simple trapezoidal integration technique, the position, velocity, and quaternion integrations are calculated.

To compensate navigation error in (1-3), an extended Kalman filter (EKF) is used with INS. In the EKF, error states are defined as (4) and system model is defined as (5).

$$\delta\mathbf{x} = [\delta L \ \delta l \ \delta h \vdots \delta v_N \ \delta v_E \ \delta v_D \vdots \delta\varphi_N \ \delta\varphi_E \ \delta\varphi_D \vdots \nabla_x \ \nabla_y \ \nabla_z \vdots \varepsilon_x \ \varepsilon_y \ \varepsilon_z]^T, \quad (4)$$

$$\delta\dot{\mathbf{x}} = \mathbf{F}_0\delta\mathbf{x} + \mathbf{w}, \ \ \mathbf{w} \sim N(0, \ \mathbf{Q}_0), \quad (5)$$

where δ indicates the error variable, δv, $\delta\varphi$, ∇, ε are the velocity error, the attitude error, the accelerometer bias, and the gyro bias, and subscript x, y, and z represent the forward, right, and vertical direction in the body frame, respectively. $\mathbf{F}_0$ is the system model matrix and described in [1], and $\mathbf{w}$ is a process noise modeled as white Gaussian with covariance $\mathbf{Q}$.

For the EKF, GPS position and velocity are used as measurements in general, as expressed in (6-8).

$$\mathbf{p}_{GPS} = \begin{bmatrix} \boldsymbol{L} & \boldsymbol{l} & \boldsymbol{h} \end{bmatrix}^T, \quad (6)$$

$$\mathbf{v}_{GPS} = \begin{bmatrix} v_N & v_E & v_D \end{bmatrix}^T, \quad (7)$$

$$\delta\mathbf{z} = \begin{bmatrix} \mathbf{p}_{INS}^T & \mathbf{v}_{INS}{}^T \end{bmatrix}^T - \begin{bmatrix} \mathbf{p}_{GPS}^T & \mathbf{v}_{GPS}{}^T \end{bmatrix}^T = [\mathbf{I}_{6\times6} \ \ \mathbf{0}_{6\times9}]\,\delta\mathbf{x}, \quad (8)$$

where $\mathbf{I}_{p\times p}$, $\mathbf{0}_{m\times n}$ represents the $p \times p$ identity matrix, and $m \times n$ zero matrix, respectively.

To correct navigation error additionally, odometer data can be used as a measurement of the filter with NHC constraint, which is used sequentially after the GPS measurement update. NHC is the constraint that the velocities which are perpendicular to forward direction of the vehicle are zero.

$$v_y^b \approx 0, \quad , v_z^b \approx 0. \quad (9)$$

The relation between body frame velocity and navigation frame velocity is described as

$$\hat{\mathbf{v}}^b = \hat{\mathbf{C}}_n^b\hat{\mathbf{v}}^n = \left(\hat{\mathbf{C}}_b^n\right)^T\hat{\mathbf{v}}^n. \quad (10)$$

By perturbing equation (10),

$$\mathbf{v}^b + \delta\mathbf{v}^b = \mathbf{C}_n^b(\mathbf{I} + (\delta\psi\times))(\mathbf{v}^n + \delta\mathbf{v}^n), \quad (11)$$

$$\delta\mathbf{v}^b \approx \mathbf{C}_n^b\delta\mathbf{v}^n + \mathbf{C}_n^b(\delta\psi\times)\mathbf{v}^n = \mathbf{C}_n^b\delta\mathbf{v}^n - \mathbf{C}_n^b(\mathbf{v}^n\times)\delta\psi. \quad (12)$$

Applying to the EKF, odometer data with NHC can be used as in (13).

$$\delta\mathbf{v}^b = \mathbf{v}_{INS} - \mathbf{v}_{meas} = \begin{bmatrix} \mathbf{0}_{3\times3} & \mathbf{C}_n^b & -\mathbf{C}_n^b(\mathbf{v}^n\times) & \mathbf{0}_{3\times3} & \mathbf{0}_{3\times3} \end{bmatrix}\delta\mathbf{x}, \quad (13)$$

$$\mathbf{v}_{meas} = \begin{bmatrix} v_x^b & v_y^b & v_z^b \end{bmatrix}^T = \begin{bmatrix} v_{odo} & 0 & 0 \end{bmatrix}^T, \tag{14}$$

where v_{odo} is an odometer speed.

B. 2D DR/GPS SYSTEM

In 2D DR/GPS, the position of the vehicle is calculated by integrating navigation frame velocity, and navigation frame velocity is calculated by speed obtained from odometer directly with heading angle as in (15-16).

$$\dot{\mathbf{p}} = \begin{bmatrix} \dot{p}_N & \dot{p}_E \end{bmatrix}^T = \mathbf{v}^n, \tag{15}$$

$$\mathbf{v}^n = \mathbf{C}_b^n \mathbf{v}^b = \begin{bmatrix} \cos\psi & -\sin\psi \\ \sin\psi & \cos\psi \end{bmatrix} \begin{bmatrix} v_{odo} \\ 0 \end{bmatrix} = \begin{bmatrix} v_{odo}\cos\psi \\ v_{odo}\sin\psi \end{bmatrix}, \tag{16}$$

where ψ is the heading angle obtained from gyro as in (3) using quaternion, and $\mathbf{C}_b^n$ means the directional cosine matrix. 2D DR/GPS position is also calculated by trapezoidal integration.

In the EKF for estimating error states, essential states include position error, velocity error, heading error and gyro bias in general as

$$\delta\mathbf{x} = [\delta p_N \ \delta p_E \vdots \delta v \vdots \delta\psi \vdots \varepsilon_z]^T. \tag{17}$$

GPS position and speed are used as measurements, as expressed in (18, 19).

$$\mathbf{p}_{GPS} = \begin{bmatrix} p_N & p_E \end{bmatrix}^T, \tag{18}$$

$$\delta\mathbf{z} = \begin{bmatrix} \mathbf{p}_{DR}^T & v_{DR} \end{bmatrix}^T - \begin{bmatrix} \mathbf{p}_{GPS}^T & v_{GPS} \end{bmatrix}^T = \begin{bmatrix} \mathbf{I}_{3\times3} & \mathbf{0}_{3\times2} \end{bmatrix} \delta\mathbf{x}. \tag{19}$$

III. MEMS 3D DR/GPS SYSTEM

3D DR/GPS system proposed in this research is composed of a navigation processor and an extended Kalman filter with sensor measurements. Filter structure of the proposed 3D DR/GPS system for navigation solution is shown in Fig. 2 with block diagram. Firstly, the DR solution is obtained by odometer and gyro, not based on accelerometer. Since odometer output is represented in body frame, its coordinate is transformed to navigation frame with transformation matrix which is calculated from attitude including roll, pitch, and yaw. In the EKF, state variables include odometer scale factor error to estimate it accurately in various environments.

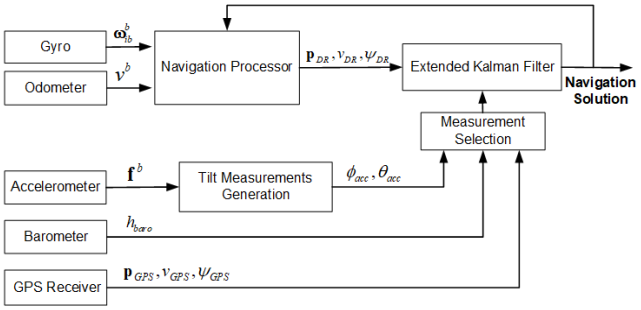

FIGURE 2. Filter structure of the proposed 3D DR/GPS system.

Accelerometer and barometer data are used as tilt (roll and pitch) measurements and altitude measurement for EKF with the same update rate of the navigation processor, respectively. GPS data is also used as measurement when it is acquired. Also, adaptation rules for measurement noise covariance are applied to improve navigation performance.

In the following section A, B, and C, the proposed 3D DR/GPS algorithm structures are introduced with equations. Also, measurement noise covariance adaptation rule is explained in section D, and the effect of estimating odometer scale factor is shown in section E.

A. NAVIGATION PROCESSOR

In the proposed 3D DR/GPS system, the position and velocity are calculated in 3D as (20-21), which are different from 2D DR/GPS equations (15-16).

$$\dot{\mathbf{p}} = \begin{bmatrix} \dot{p}_N & \dot{p}_E & \dot{p}_D \end{bmatrix}^T = \mathbf{v}^n, \tag{20}$$

$$\mathbf{v}^n = \mathbf{C}_b^n \mathbf{v}^b = \mathbf{C}_b^n \begin{bmatrix} v_{odo} & 0 & 0 \end{bmatrix}^T = \mathbf{C}_b^n \begin{bmatrix} s\,u_{odo} & 0 & 0 \end{bmatrix}^T, \tag{21}$$

where u_{odo} and s are odometer output and odometer scale factor, respectively. In this model, odometer scale factor s is modelled using multiplicative error model as $s(1+\delta s)$, whose nominal value is s.

Attitude update in (3) that uses quaternion is employed in the navigation processor since 3D DR/GPS system also uses gyro in attitude calculation.

B. DERIVATION OF 3D DR/GPS SYSTEM ERROR MODEL

The proposed error compensation algorithm in 3D DR/GPS is based on EKF, and following models are described below.

Process model of the navigation error equation is described in (22).

$$\delta\dot{\mathbf{x}} = \mathbf{F}\delta\mathbf{x} + \mathbf{w}, \ \ \mathbf{w} \sim N(0, \ \mathbf{Q}), \tag{22}$$

where $\mathbf{w}$ is a process noise modeled as white Gaussian with covariance $\mathbf{Q}$.

State variables of the proposed filter are position error, odometer scale factor error, attitude error, and gyro bias as expressed in (23).

$$\delta\mathbf{x} = [\delta p_N \ \delta p_E \ \delta p_D \vdots \delta s \vdots \delta\varphi_N \ \delta\varphi_E \ \delta\varphi_D \vdots \varepsilon_x \ \varepsilon_y \ \varepsilon_z]^T, \tag{23}$$

where δp, δs, $\delta\varphi$, ε are the position error, the odometer scale factor error, the attitude error, and the gyro bias, respectively. Velocity error in INS/GPS system is replaced by odometer scale factor, and accelerometer bias term is removed because accelerometer is not used for calculating velocity but as EKF measurement for tilt error compensation. Since the accelerometer is not used for obtaining velocity, it does not directly induce position error. In addition, the accelerometer bias is initially corrected, and so that residual bias of less than 10% has remained [46]. Noting that the turn-on bias of SMI 130 accelerometer is less than 70 mg and the temperature coefficient is less than 1mg/K, we can assume the residual

bias will be kept smaller than 7 mg for 1 hour. The residual bias influences on the measurement quality, which is not significant compared with other error sources.

Derivative of position estimate in navigation frame can be represented with transformation of the velocity in body frame as in (24),

$$\dot{\hat{\mathbf{p}}} = \hat{\mathbf{C}}_b^n \hat{\mathbf{v}}^b = (\mathbf{I} - (\delta\psi\times))\mathbf{C}_b^n(\mathbf{v}^b + \delta\mathbf{v}^b), \quad (24)$$

$$\delta\mathbf{v}^b = \begin{bmatrix}\delta v_{odo} & 0 & 0\end{bmatrix}^T, \quad (25)$$

$$\delta v_{odo} = \delta s \times u_{odo}, \quad (26)$$

where $\hat{\mathbf{p}}$, $\hat{\mathbf{C}}_b^n$, $\hat{\mathbf{v}}^b$ are the outputs of pure navigation algorithm and $(\delta\psi\times)$ skew-symmetric matrix representing the vector cross product by the vector $\delta\psi$.

Position error model is obtained in (27) using (20), (21) and (24), and eliminating second order term. The speed is assumed to have only x directional value of the vehicle like NHC assumption.

$$\delta\dot{\mathbf{p}} = \dot{\hat{\mathbf{p}}} - \dot{\mathbf{p}} = \hat{\mathbf{C}}_b^n\hat{\mathbf{v}}^b - \mathbf{C}_b^n\mathbf{v}^b \approx \mathbf{C}_b^n\delta\mathbf{v}^b - (\delta\psi\times)\mathbf{v}^n. \quad (27)$$

This equation is the same as NHC equation (12) when substituting $\delta\dot{\mathbf{p}} = \delta\mathbf{v}^n$. Since the assumption with zero speed along y, z axis in (12) is the same as the results in (27) where the second order term is eliminated, using (27) means NHC is applied directly to the 3D DR/GPS system.

To use position error model in the filter, (27) can be expressed as alternate form, (28).

$$\delta\dot{\mathbf{p}} = \mathbf{C}_b^n\delta\mathbf{v}^b + (\mathbf{v}^n\times)\delta\psi = \mathbf{C}_b^n\begin{bmatrix}1 & 0 & 0\end{bmatrix}^T\delta s \times u_{odo} + (\mathbf{v}^n\times)\delta\psi. \quad (28)$$

Odometer scale factor error and gyro bias are modelled as first order Markov process model, as shown in (29)

$$\begin{cases}\delta\dot{s} = -\dfrac{1}{\tau_1}\delta s + n_s \\ \delta\dot{\varepsilon} = -\dfrac{1}{\tau_2}\delta\varepsilon + n_\varepsilon,\end{cases} \quad (29)$$

where τ_1, τ_2 are the time constants.

Since the proposed algorithm estimates odometer scale factor, it can estimate odometer velocity exactly even if odometer scale factor is set wrong initially or varies over time. Since a vehicle moves dynamically, we use the odometer scale factor error model instead of odometer bias error model.

From (28) and (29), the system matrix $\mathbf{F}$ of the 3D DR/GPS error equation is expressed by (30), and its submatrices are expressed by (31, 32).

$$\mathbf{F} = \begin{bmatrix} \mathbf{0}_{3\times3} & \mathbf{C}_b^n\begin{bmatrix}u_{odo}\\0\\0\end{bmatrix} & \left(\mathbf{C}_b^n\begin{bmatrix}su_{odo}\\0\\0\end{bmatrix}\times\right) & \mathbf{0}_{3\times3} \\ \mathbf{0}_{1\times3} & -\dfrac{1}{\tau_1} & \mathbf{0}_{1\times3} & \mathbf{0}_{1\times3} \\ \mathbf{F}_{31} & \mathbf{0}_{3\times1} & \mathbf{F}_{33} & -\mathbf{C}_b^n \\ \mathbf{0}_{3\times3} & \mathbf{0}_{3\times1} & \mathbf{0}_{3\times3} & -\dfrac{1}{\tau_2}\mathbf{I}_{3\times3} \end{bmatrix}, \quad (30)$$

$$\mathbf{F}_{31} = \begin{bmatrix} \dfrac{1}{R_m+h}(\Omega_D - \dfrac{\rho_N R_{tt}}{R_t+h}) & 0 & -\dfrac{\rho_N}{R_t+h} \\ -\dfrac{\rho_E R_{mm}}{(R_m+h)^2} & 0 & -\dfrac{\rho_E}{R_m+h} \\ \dfrac{1}{R_m+h}(-\Omega_N - \rho_N\sec^2 L - \dfrac{\rho_D R_{tt}}{R_t+h}) & 0 & -\dfrac{\rho_D}{R_t+h} \end{bmatrix}, \quad (31)$$

$$\mathbf{F}_{33} = \begin{bmatrix} 0 & \Omega_D + \rho_D & -\rho_E \\ -\Omega_D - \rho_D & 0 & \Omega_N + \rho_N \\ \rho_E & -\Omega_N - \rho_N & 0 \end{bmatrix}, \quad (32)$$

where $\mathbf{0}_{m\times n}$ represents the $m \times n$ zero matrix.

C. EXTENDED KALMAN FILTER WITH SENSOR MEASUREMENTS

To compensate navigation errors, an EKF is applied to the error model (22). In this study, position, ground speed and course angle from GPS, barometer data, and attitude calculated by acceleration are used to compensate errors. Since the sampling rates of measurements are different, measurement update of the EKF is divided into two steps. In step 1, the measurement update for attitude error and barometric altitude error compensation is done at 20 Hz rate. In this stage, tilt angle from accelerometer and barometer are used as measurements. Then in step 2, measurement update using GPS position, ground speed, and course angle is done at 1 Hz rate for mainly compensating position error, height error, azimuth error, and odometer scale factor error. In both steps, the measurement equation of the Kalman filter is expressed as

$$\delta\mathbf{z} = \mathbf{H}\delta\mathbf{x} + \boldsymbol{\eta}, \quad \boldsymbol{\eta} \sim N(0,\ \mathbf{R}), \quad (33)$$

where $\boldsymbol{\eta}$ is the white Gaussian measurement noise with covariance R.

In step 1, tilt measurements are used, which are converted from the accelerometer measurement. If the navigation processor explained in section III-A is only working in the vehicle, attitude error is accumulated over time. While GPS data cannot compensate the attitude of the vehicle at GPS outage area, step 1, which can be used in GPS outage area, can correct tilt of the vehicle and play an important role for improving navigation performance. Tilt measurements can be generated by accelerometer output using (34, 35), and they are used for tilt angle correction in step 1 [11]. Since the residual bias of less than 7mg ($= 0.07\text{m/s}^2$) contributes to the tilt angle errors by only 0.4011deg, the residual accelerometer bias after initial calibration influences little on the measurement quality compared with other error sources such as engine vibration, vibration during driving due to the road condition, and other dynamic errors.

$$\phi_{acc} = \tan^{-1}\left(\frac{f_y}{f_z}\right), \quad (34)$$

$$\theta_{acc} = \tan^{-1}\left(\frac{f_x}{\sqrt{f_y^2+f_z^2}}\right), \quad (35)$$

where f_x, f_y, f_z are the accelerometer outputs.

However, (34, 35) become inaccurate in high dynamic cases since additional accelerations are applied. To solve the problem, active compensation of the tilt angles, which estimates applied acceleration and uses the compensated acceleration for calculating tilt angles, can be applied to (34, 35) as presented in the RISS/GPS [34]–[37]. In this case, however, the calculated tilt angle cannot be used for EKF measurements because they are correlated with other error states. Therefore, the calculated tilt angles are directly used for the navigation process. Since noisy acceleration is included in active compensation, using it directly for tilt angle calculation causes inaccurate results compared with gyro quaternion based method used in this research.

Another effective solution to the problem is using adaptation rule for measurement update. The proposed 3D DR/GPS uses this method, and it will be explained in section III-D.

Also, altitude obtained from barometer is combined together in step 1 since sampling rates of the barometer and the accelerometer are the same in the proposed system. Therefore, the measurement update equation in step 1 is summarized as

$$\begin{aligned}\delta \mathbf{z}_1 &= \mathbf{H}_1 \delta \mathbf{x} + \boldsymbol{\eta}_1 \\ &= \begin{bmatrix} \phi_{DR} & \theta_{DR} & h_{DR} \end{bmatrix}^T - \begin{bmatrix} \phi_{acc} & \theta_{acc} & h_{baro} \end{bmatrix}^T, \end{aligned} \tag{36}$$

$$\mathbf{H}_1 = \begin{bmatrix} \mathbf{0}_{1\times 4} & \begin{bmatrix} -\frac{\cos\psi}{\cos\theta} & -\frac{\sin\psi}{\cos\theta} & 0 \end{bmatrix} & \mathbf{0}_{1\times 3} \\ \mathbf{0}_{1\times 4} & \begin{bmatrix} \sin\psi & -\cos\psi & 0 \end{bmatrix} & \mathbf{0}_{1\times 3} \\ \begin{bmatrix} 0 & 0 & 1 & 0 \end{bmatrix} & \mathbf{0}_{1\times 3} & \mathbf{0}_{1\times 3} \end{bmatrix}, \tag{37}$$

where subscript 1 represents the step 1, subscript DR represents the dead reckoning output, and ψ is the yaw angle.

In step 2, GPS position, ground speed, and heading angle are used as measurements to compensate odometer scale factor error and azimuth angle, as expressed in (38-41). The GPS heading values are provided from the GPRMC information in the NMEA log. Covariance of the EKF state is updated by step 1 at 20Hz, and updated one more time by step 2 at 1Hz.

$$\mathbf{p}_{GPS} = \begin{bmatrix} p_N & p_E & p_D \end{bmatrix}^T, \tag{38}$$

$$v_{DR} = s u_{odo}, \tag{39}$$

$$\begin{aligned}\delta \mathbf{z}_2 &= \mathbf{H}_2 \delta \mathbf{x} + \boldsymbol{\eta}_2 \\ &= \begin{bmatrix} \mathbf{p}_{DR}^T & v_{DR} & \psi_{DR} \end{bmatrix}^T - \begin{bmatrix} \mathbf{p}_{GPS}^T & v_{GPS} & \psi_{GPS} \end{bmatrix}^T, \end{aligned} \tag{40}$$

$$\mathbf{H}_2 = \begin{bmatrix} \mathbf{I}_{3\times 3} & \mathbf{0}_{3\times 1} & \mathbf{0}_{3\times 3} & \mathbf{0}_{3\times 3} \\ \mathbf{0}_{1\times 3} & u_{odo} & \mathbf{0}_{1\times 3} & \mathbf{0}_{1\times 3} \\ \mathbf{0}_{1\times 3} & 0 & \begin{bmatrix} \tan\theta\cos\psi & \tan\theta\sin\psi & -1 \end{bmatrix} & \mathbf{0}_{1\times 3} \end{bmatrix}. \tag{41}$$

To compensate height error, both GPS height and barometer are used as measurements selectively as shown in (36) and (40). In open sky, GPS height is used to adjust barometer bias simply, and both GPS height and barometer are used as significant measurements for height error compensation. Since GPS height is not reliable around urban canyons, or not available in GPS outage area, it is selectively used only when GPS quality is good. In GPS outage area or around urban canyons where GPS condition is not good enough, it is examined that the GPS height may have fatal error more than 19m. Therefore, barometer height, whose bias is adjusted already, is mainly used alternatively in this situation.

D. ADAPTATION RULE FOR MEASUREMENT NOISE COVARIANCE

To improve navigation accuracy, three measurement noise covariance adaptation rules are applied.

First part is checking the accuracy of the attitude measurements by measuring accelerometer disturbances, which was described earlier in measurement update step 1 of the section C. Since (34, 35) are appropriate only for static situation, they cannot be used when the norm of the acceleration $\|\mathbf{f}\|$ is not within reliable boundary [11]. So, if $\|\mathbf{f}\|$ is considerably larger than the pre-determined boundary, which means that $\|\mathbf{f}\| - \mathbf{g}$ is larger than the threshold, the measurement noise covariance related to the attitude error, $\mathbf{R}_a$, should be increased. If the threshold is set too high, attitude measurement form (34, 35) will be used for all cases with low $\mathbf{R}_a$, which degrades navigation performance. On the contrary, when threshold is set too low, attitude measurement may be used with high $\mathbf{R}_a$ even in static situation, meaning that the measurement will not be used properly for compensating tilt error. So it is important to choose appropriate threshold.

The threshold is determined from MATLAB simulations. It is assumed that the vehicle is driven along the 2-dimensional curved course for 500 seconds and speed is constant as 20 m/s except start and end point. Specification of the MEMS IMU is same as in TABLE 1 of section IV-A, which will be explained later with experiment data.

Using the simulation data, the accuracy of tilt measurement is checked according to the norm of acceleration, and this relationship is shown in Fig. 3. The blue shaded area is the section where the vehicle makes turn and the norm of the acceleration increases. Firstly, we checked the points where the roll or pitch angle error becomes larger than 5 degrees, which are indicated by red circles in the figure. At those

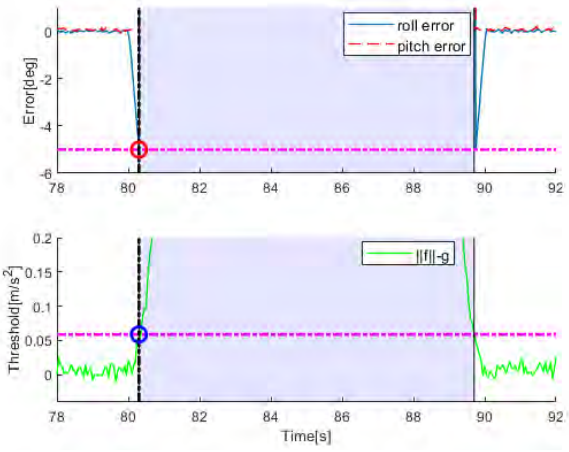

FIGURE 3. Relation between attitude calculated by accelerometer and norm of the acceleration.

points, the value of $\|\mathbf{f}\| - \mathbf{g}$ can be obtained as blue circle point, which indicates $0.059\,m/s^2 \approx 0.006\,g$. By this result, we chose the threshold for vehicle experiment.

Second part is deciding the reliability of Doppler measurements according to vehicle speed. Since Doppler quality degrades as the vehicle speed becomes lower [28], GPS velocity measurement noise covariance $\mathbf{R}_g$ should be adapted according to the vehicle speed. In the experiment of section IV, vehicle speed was measured by odometer and shown in Fig. 4. Shaded areas in Fig. 4 are the low velocity section with retaining similar speed for a long time, and we selected threshold for classifying low speed section and high speed section near these values, which is approximately $4 \sim 6\ m/s$.

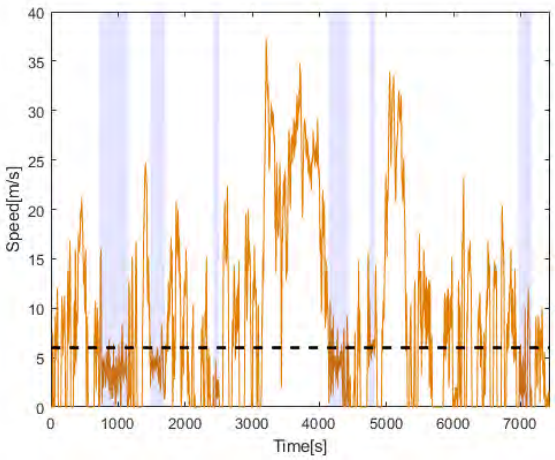

FIGURE 4. Vehicle speed measured by odometer.

Lastly, adaptation is also applied to height error estimation. Barometric height measurement can be changed rapidly due to pressure change by opening window of the vehicle. Thus, the innovation based adaptation rule is applied to height error estimation. If the difference of the estimated height and barometric height measurement is larger than threshold, the measurement is judged to be inaccurate, and the adaptation rule increases the measurement noise covariance related to the height error. The threshold is set near to 2.5 m, which is almost 80 % of one floor height.

E. EFFECT OF ESTIMATING ODOMETER SCALE FACTOR

Since the odometry error induces position error directly in the 3D DR/GPS, it should be pre-determined or estimated accurately. However, it cannot be easily determined because it relies on tire conditions and varies over time. Thus, odometer scale factor error is included in the error state vector for exact estimation using GPS speed measurement. The importance of odometer scale factor error estimation is validated by MATLAB simulation with the same scenario in section D. Firstly, the effect of initial odometer scale factor error is examined when the odometer scale factor is not estimated in DR/GPS system. Estimated trajectories according to various odometer scale factors are compared in Fig. 5, and they show the

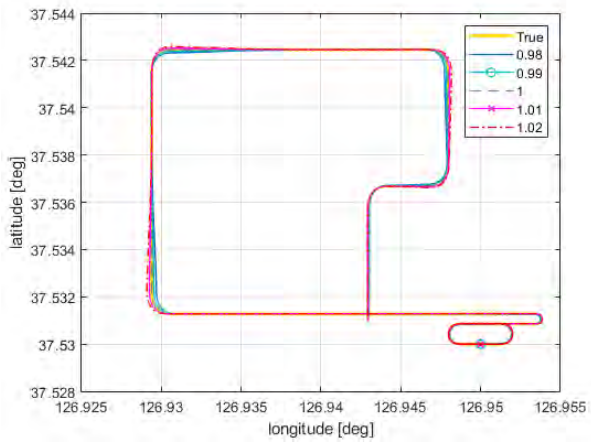

FIGURE 5. Estimated trajectory according to different odometer scale factor.

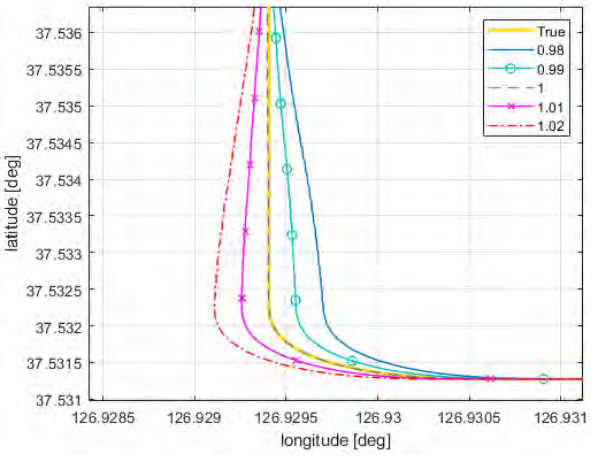

FIGURE 6. Effect of wrong odometer scale factor in curved course.

differences at curved courses. True odometer scale factor value was set to 1, and multiplicative error model is used. The lower left corner of Fig. 5 is magnified in Fig. 6. The vehicle goes left and turns right at the corner. When odometer scale factor is set smaller than 1, it turns inside of the corner, and turns outside in opposite case even when position measurements from GPS receiver are available.

Figs. 7 and 8 are attitude and position errors with constant odometer scale factor. Yellow bars in the figures mean curved courses. Since roll and pitch angles are compensated by the filter as explained in the previous sections III-C and D, they are not affected by odometer scale factor error. However, odometer scale factor error induces yaw error at curved courses because the filter tries to compensate the difference between the position by the odometer and GPS position measurement, which also increases position error.

By estimating odometer scale factor, these problems can be solved. Fig. 9 shows the estimation results of odometer scale factor errors using the proposed 3D DR/GPS system. Since the estimate of scale factor converges to true value 1,

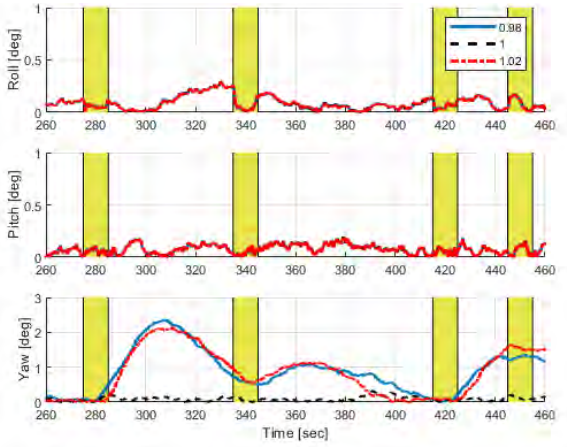

FIGURE 7. Attitude error according to different initial odometer scale factor.

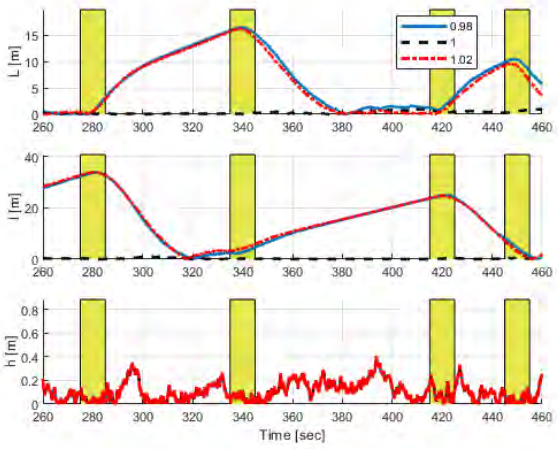

FIGURE 8. Position error according to different initial odometer scale factor.

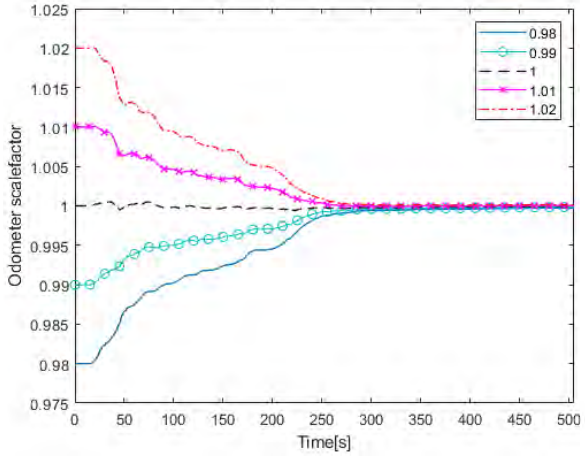

FIGURE 9. Estimate of odometer scale factor using 3D DR/GPS system.

attitude and position errors are sustained small and show stable performance regardless of initial odometer scale factor errors as shown in Figs. 10 and 11.

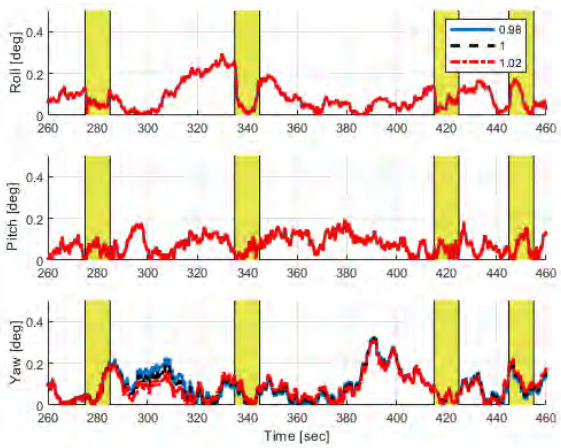

FIGURE 10. Attitude error according to different initial odometer scale factor using 3D DR/GPS system.

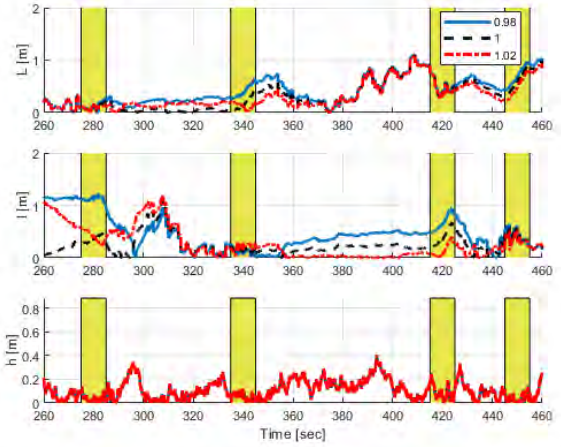

FIGURE 11. Position error according to different initial odometer scale factor using 3D DR/GPS system.

IV. PERFORMANCE EVALUATION

To validate the proposed algorithm, several vehicle tests were conducted. Test settings and results are described in this section.

A. TEST SETTINGS

Several experimental tests with vehicle were conducted to verify the proposed algorithm. Data acquisition modules used in the experiment were installed at the interior of the vehicle, which is shown in Fig. 12. Experimental equipment and data acquisition were supported by Hyundai MnSOFT. These modules include 6-axis inertial sensor, SMI 130, by Bosch that provides navigation data. In addition, GNSS receiver STA8089FG by STMicroelectronics and barometer BMP 280 by Bosch were used. All the specifications are summarized in Table 1 and 2.

The vehicle tests were performed several times on urban area including GPS outage section as shown in Fig. 13. Total experiment time for one test was about 7,440 seconds, length was 64.56 km, and speed measured by odometer is shown

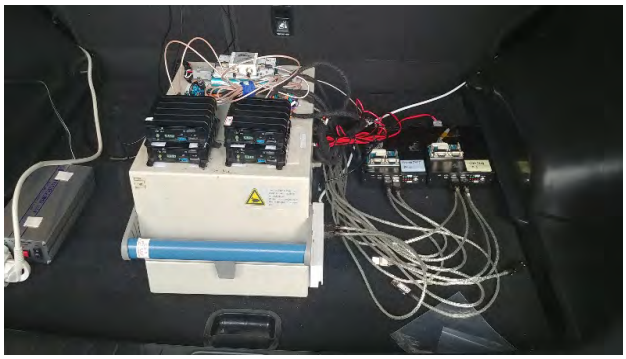

FIGURE 12. Data acquistion module mounted behind the vehicle.

FIGURE 13. Test trajectory.

TABLE 1. Specification of the inertial sensors.

	SMI 130 gyro	SMI 130 accelerometer
Zero-point offset	$\pm 1\,\mathrm{deg}/\,s$	$\pm 70\,mg$
Temperature coeffecint	$\pm 0.015\,\mathrm{deg}/\,s\,/\,K$	$\pm 1mg\,/\,K$
RMS Noise	$0.02\,\mathrm{deg}/\,s\,/\sqrt{Hz}$	$0.19\,\mathrm{mg}/\sqrt{Hz}$
Sampling rate	$20\,Hz$	$20\,Hz$

TABLE 2. Specification of the barometer.

	BMP 280
Pressure range	$300 \sim 1100\,hPa$
RMS Noise	$1.3\,Pa$
Sampling rate	$20\,Hz$

in Fig. 4. To analyze the navigation accuracy of the proposed system, estimated trajectory at open sky and three GPS outage areas were considered in next section.

B. TEST RESULTS

Since the GPS horizontal position is used for position measurements in the open sky area, the position error is bounded by the GPS position. Fig. 14 shows the results in the open sky area and the proposed algorithm provides position with bounded error. In this area, we factitiously blocked GPS

FIGURE 14. Factitiously block GPS in open sky.

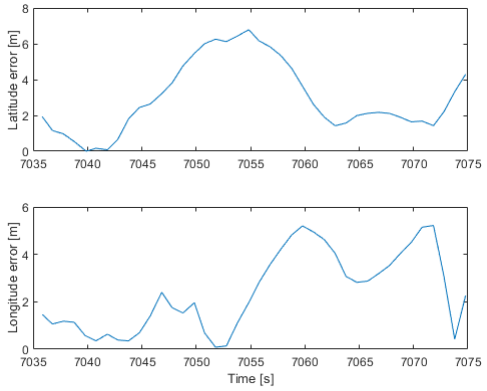

FIGURE 15. Position error with factitiously block GPS in open sky.

data for 40 seconds and compared the proposed 3D DR/GPS solution with GPS position data. Even for this case, the proposed algorithm provided stable horizontal position without divergence as shown in Fig. 15. If conventional algorithm is employed, the error will increase monotonically with time. However, the proposed 3D DR/GPS uses measurement update using tilt measurement and barometer even when GPS is not available. Therefore, the error does not simply diverge with time, but fluctuates within some bound. The fluctuation in position error is mainly caused by tilt angle measurement because tilt correction influences on azimuth angle, which results in position change. Moreover, the test site was interchange with relatively large tilt angle, so that tilt correction influences more on position change. As shown in the Figure, the horizontal error does not diverge and is bounded under 7 m, which is similar to the accuracy of the GPS horizontal position.

Estimated trajectories in GPS outage areas are shown in Figs. 16 to 18. In these areas, map information provided by Google satellite map in MATLAB was used as a reference since it provides accurate position and align direction of buildings and roads. The accuracy of the Google satellite map in the region where the vehicle tests were conducted was validated against the map created by the Hyundai MnSOFT, which has an accuracy of 3∼4m, globally. However, since the map error appears in the form of a bias in a small area, it can be seen that the map is relatively more accurate than 3∼4m when calculating the navigation error.

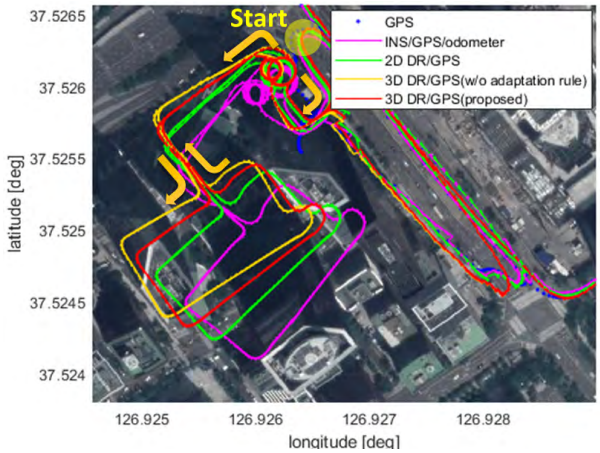

FIGURE 16. GPS outage area 1: underground parking garage (409 s).

Conventional 2D DR/GPS and conventional INS/GPS/odometer algorithm with odometer are also compared with the proposed algorithm. Fig. 16 shows the results in the underground parking lot course with GPS outage of 409 seconds. It starts with going down rotating downhill and after passing several turning course in the underground, going up rotating uphill at the end. The shape of the underground course by the proposed algorithm is well-aligned with the buildings in the satellite map, and each circle shape corresponds to a circular rotation section. Also, by comparing with 3D DR/GPS without adaptation rule, it can be confirmed that the proposed adaptation rule is important to accurately estimate the attitude. On the other hand, heading angle error of the 2D DR/GPS increases after downhill since it does not consider tilt angles, which results in the distorted and misaligned trajectory with buildings. Also, the NHC, used in the 2D DR/GPS, and heading error may cause unexpected position error when the vehicle rotates repeatedly as shown in Table 3.

TABLE 3. Position errors in GPS outage areas.

		INS/GPS /odometer (m)	2D DR/GPS (m)	3D DR/GPS (Proposed, m)
Dataset 1	Area 1 (409 s)	23.69	13.72	10.72
	Area 2 (182 s)	24.20	9.60	0.87
Dataset 2	Area 1 (314 s)	92.83	20.37	7.97
	Area 2 (201 s)	26.44	21.93	13.73

INS/GPS/odometer shows more errors compared to 2D DR/GPS since the velocity error induced by accelerometers' bias is larger than odometer error as explained. Fig. 17 presents the results in a multilevel parking garage with 182 seconds GPS outage. Opposite to the case shown in Fig. 16, it starts with going up the rotating section and after passes turning course at the rooftop, it goes down the rotation section. The proposed algorithm also shows a

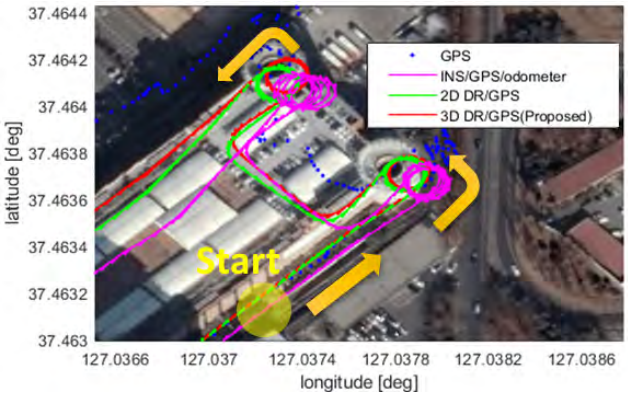

FIGURE 17. GPS outage area 2: multilevel parking garage (182 s).

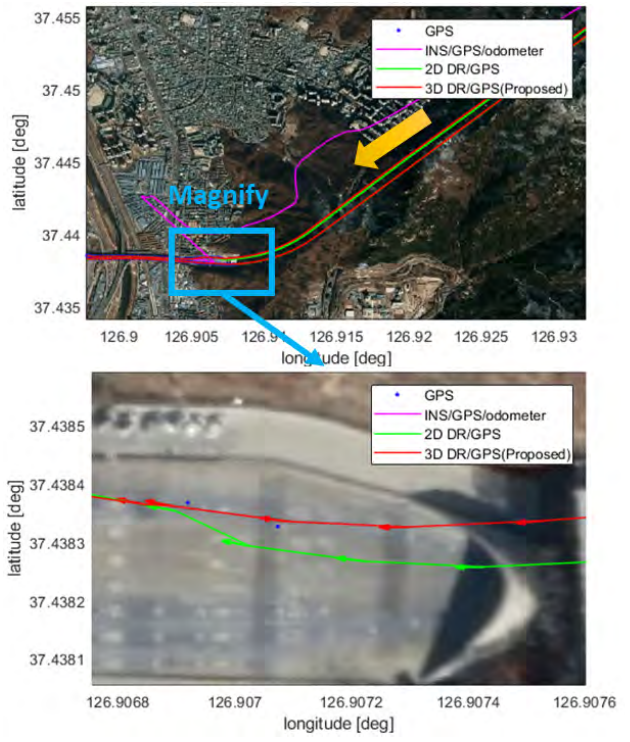

FIGURE 18. GPS outage area 3: tunnel with smooth curve (159 s).

well-aligned trajectory in this area. 2D DR/GPS shows heading error at the end of the trajectory, and a circular section of INS/GPS/odometer is distorted due to velocity error and attitude error. Fig. 18 shows the results in a tunnel section with a smooth curve, and it lasts for 159 seconds. In this area, position error was calculated after the vehicle came out of the tunnel. In this case, position error was 1.91 m using the proposed algorithm, and 5.74 m using 2D DR/GPS. INS /GPS/odometer result showed bad performance since the attitude was not compensated correctly.

Position errors of the three algorithms on the GPS outage sections where the GPS is not available for more than 3 minutes are summarized in Table 3. The errors were calculated based on the closest point of the road segment.

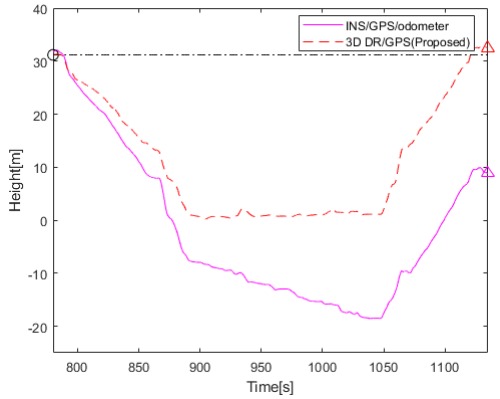

FIGURE 19. Height estimate from entrance to exit of underground parking garage.

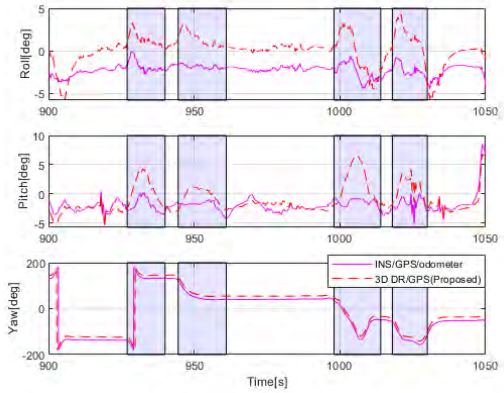

FIGURE 20. Attitude estimate at underground parking garage.

The proposed algorithm showed smaller position errors than other two algorithms.

Because there is no reliable reference for altitude, altitude change at the same point where the underground parking garage starts and ends (Fig. 16) is calculated for error analysis. Since 2D DR/GPS does not provide height when GPS is not available, 3D DR/GPS and INS/GPS/odometer are compared in Fig. 19. Height estimate of the 3D DR/GPS changed only 1.22 m, but that of INS/GPS/odometer changed 22.34 m. This difference is caused by an estimation error of pitch angle. Fig. 20 shows the results for estimated attitude at the flatland of the underground parking lot. Since true attitude cannot be easily acquired when GPS is not available, we focus more on the fluctuated values than the average value in analyzing attitude error. In Fig. 20, shaded areas present the location where speed bumps exist. In these area, pitch angle should go up and down. The proposed algorithm reflects the effect of speed bumps at the shaded area, but the pitch of INS/GPS/odometer is not affected enough.

Fig. 21 shows the comparison results of 3D RISS/GPS and 3D DR/GPS at a tunnel. The position errors of 3D RISS/GPS, 3D DR/GPS are 24.56m and 20.86m, respectively. As shown in the figure, the estimation performance of 3D DR/GPS is more accurate than 3D RISS/GPS.

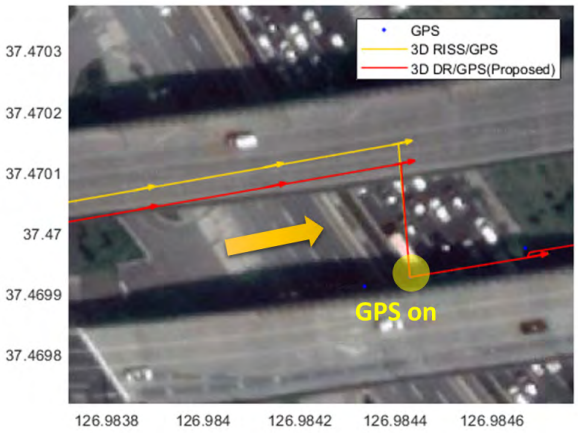

FIGURE 21. GPS outage area 4: tunnel with smooth curve (132 s).

V. CONCLUSION

In this research, MEMS IMU based 3D DR/GPS system was proposed, and performance was verified with vehicle tests. To improve the performance, INS/GPS system was substituted to DR/GPS algorithm, which is less affected by large bias error of accelerometer, and 3D navigation solution was suggested to reduce error in uphill and downhill more effectively than conventional 2D DR/GPS system. To compensate navigation errors, the error model and measurement equations for 3D DR/GPS was derived and EKF was applied. Especially, odometer scale factor was estimated and its necessity was verified by MATLAB simulation. Also, adaptation rules for measurement noise covariance were applied to use measurement information appropriately. In vehicle tests, the proposed 3D DR/GPS system provided a more reliable navigation solution than conventional 2D DR/GPS and INS/GPS/odometer systems because the proposed algorithm estimated attitude and 3D position more effectively and used attitude and altitude measurements as well as GPS measurements. In result, the proposed algorithm showed smaller position errors than other two algorithms.

The proposed method improved the estimation performance of MEMS-based navigation system without additional bulky hardware for the vehicle. It showed stable estimation performance for long GPS outage time, when a low-cost MEMS-based navigation system is vulnerable to diverge. In addition, it estimates odometer scale factor, so that it is applicable to various vehicles with unknown different odometer scale factor. Therefore, the proposed method can be used for any navigation system that needs low-cost simple navigation system, but requires robust performance for GPS outage.

ACKNOWLEDGMENT

(Woo Jung Park and Jin Woo Song contributed equally to this work.)

REFERENCES

[1] D. H. Titterton and J. L. Weston, *Strapdown Inertial Navigation Technology*, 2nd ed. Stevenage, U.K.: IET, 2004.

[2] P. D. Groves, *Principles of GNSS, Inertial, and Multisensor Integrated Navigation Systems*, 2nd ed. Norwood, MA, USA: Artech House, 2013.

[3] J. Seo, H. K. Lee, J. G. Lee, and C. G. Park, "Lever arm compensation for GPS/INS/odometer integrated system," *Int. J. Control, Autom., Syst.*, vol. 4, no. 2, pp. 247–254, Apr. 2006.

[4] J. Park, D. S. Lee, and C. Park, "Implementation of vehicle navigation system using GNSS INS odometer and barometer," *J. Positioning, Navigat., Timing*, vol. 4, no. 3, pp. 141–150, 2015.

[5] J. A. Farrel and M. Barth, *The Global Positioning System & Inertial Navigation*. New York, NY, USA: McGraw-Hill, 1999.

[6] K. Kim, C. G. Park, and M. J. Yu, "Adaptive Kalman filter for the navigation system with virtual velocity measurement," in *Proc. Eur. Control Conf. (ECC)*, Jul. 2007, pp. 2207–2212.

[7] Y. M. Yoo, J. G. Park, D. H. Lee, and C. G. Park, "A theoretical approach to observability analysis of the SDINS/GPS in maneuvering with horizontal constant velocity," *Int. J. Control, Autom. Syst.*, vol. 10, no. 2, pp. 298–307, Apr. 2012.

[8] Y. Zhang, C. Shen, J. Tang, and J. Liu, "Hybrid algorithm based on MDF-CKF and RF for GPS/INS system during GPS outages," *IEEE Access*, vol. 6, pp. 35343–35354, 2018.

[9] G. Falco, M. Nicola, and M. Pini, "Positioning based on tightly coupled multiple sensors: A practical implementation and experimental assessment," *IEEE Access*, vol. 6, pp. 13101–13116, 2018.

[10] S. Godha and M. E. Cannon, "GPS/MEMS INS integrated system for navigation in urban areas," *GPS Solutions*, vol. 11, no. 3, pp. 193–203, Jul. 2007.

[11] D. Won, J. Ahn, S. Sung, M. Heo, S. H. Im, and Y. J. Lee, "Performance improvement of inertial navigation system by using magnetometer with vehicle dynamic constraints," *J. Sensors*, vol. 2015, Jul. 2015, Art. no. 435062.

[12] A. Kealy, S. Scott-Young, F. Leahy, and P. Cross, "Improving the performance of satellite navigation systems for land mobile applications through the integration of MEMS inertial sensors," in *Proc. 14th Int. Tech. Meeting Satell. Division Inst. Navigat. (ION-GPS)*, Sep. 2001, pp. 1394–1402.

[13] A. Noureldin, T. B. Karamat, M. D. Eberts, and A. El-Shafie, "Performance enhancement of MEMS-based INS/GPS integration for low-cost navigation applications," *IEEE Trans. Veh. Technol.*, vol. 58, no. 3, pp. 1077–1096, Mar. 2009.

[14] H. Liu, Z. Wang, S. Fang, and C. Li, "MEMS based SINS/OD filter for land vehicles' applications," *Math. Problems Eng.*, vol. 2017, Jan. 2017, Art. no. 1691320.

[15] A. Wahdan, J. Georgy, W. F. Abdelfatah, and A. Noureldin, "Magnetometer calibration for portable navigation devices in vehicles using a fast and autonomous technique," *IEEE Trans. Intell. Transp. Syst.*, vol. 15, no. 5, pp. 2347–2352, Oct. 2014.

[16] A. Abosekeen, A. Noureldin, T. Karamat, and M. J. Korenberg, "Comparative analysis of magnetic-based RISS using different MEMS-based sensors," in *Proc. 30th Int. Tech. Meeting Satell. Division Inst. Navigat. (ION GNSS)*, Sep. 2017, pp. 2944–2959.

[17] Y. Kim and D.-W. Hwang, "Vision/INS integrated navigation system for poor vision navigation environments," *Sensors*, vol. 16, no. 10, p. 1672, 2016.

[18] Y. S. Kim and D. H. Hwang, "Loosely-coupled vision/INS integrated navigation system," *J. Positioning, Navigat., Timing*, vol. 6, no. 2, pp. 59–70, 2017.

[19] S. Kim and J.-H. Kim, "Adaptive fuzzy-network-based C-measure map-matching algorithm for car navigation system," *IEEE Trans. Ind. Electron.*, vol. 48, no. 2, pp. 432–441, Apr. 2001.

[20] D. Bétaille, F. Peyret, M. Ortiz, S. Miquel, and L. Fontenay, "A new modeling based on urban trenches to improve GNSS positioning quality of service in cities," *IEEE Intell. Transp. Syst. Mag.*, vol. 5, no. 3, pp. 59–70, Jul. 2013.

[21] Y. Kim, J. An, and J. Lee, "Robust navigational system for a transporter using GPS/INS fusion," *IEEE Trans. Ind. Electron.*, vol. 65, no. 4, pp. 3346–3354, Apr. 2018.

[22] X. Li and Q. Xu, "A reliable fusion positioning strategy for land vehicles in GPS-denied environments based on low-cost sensors," *IEEE Trans. Ind. Electron.*, vol. 64, no. 4, pp. 3205–3215, Apr. 2017.

[23] X. Wang, J. X. Chen, and W. Ni, "A hybrid prediction method and its application in the distributed low-cost INS/GPS integrated navigation system," in *Proc. 18th Int. Conf. Inf. Fusion (Fusion)*, Jul. 2015, pp. 1205–1212.

[24] B.-H. Lee, J.-H. Song, J.-H. Im, S.-H. Im, M.-B. Heo, and G.-I. Jee, "GPS/DR error estimation for autonomous vehicle localization," *Sensors*, vol. 15, no. 8, pp. 20779–20798, Aug. 2015.

[25] Y. Xiaoyun and H. Heng, "GPS/DR integrated navigation system based on adaptive robust Kalman filtering," in *Proc. Int. Conf. Microw. Millim. Wave Technol.*, vol. 4, Apr. 2008, pp. 1946–1949.

[26] R. Guo, P. Xiao, L. Han, and X. Cheng, "GPS and DR integration for robot navigation in substation environments," in *Proc. IEEE Int. Conf. Inf. Automat.*, Jun. 2010, pp. 2009–2012.

[27] H. Zhang and Y. Zhao, "The performance comparison and analysis of extended Kalman filters for GPS/DR navigation," *Optik*, vol. 122, no. 9, pp. 777–781, May 2011.

[28] J. H. Song, K. H. Kim, G. I. Jee, and Y. S. Lee, "Performance improvement of GPS/DR car navigation system using vehicle movement," *Inf. J. Korea Robot. Soc.*, vol. 5, no. 1, pp. 55–63, 2010.

[29] H. Ahmed and M. Tahir, "Accurate attitude estimation of a moving land vehicle using low-cost MEMS IMU sensors," *IEEE Trans. Intell. Transp. Syst.*, vol. 18, no. 7, pp. 1723–1739, Jul. 2017.

[30] M. T. Sabet, H. R. M. Daniali, A. R. Fathi, and E. Alizadeh, "Experimental analysis of a low-cost dead reckoning navigation system for a land vehicle using a robust AHRS," *Robot. Auton. Syst.*, vol. 95, pp. 37–51, Sep. 2017.

[31] J.-H. Han, C.-H. Park, C.-K. Hong, and J. H. Kwan, "Performance analysis of two-dimensional dead reckoning based on vehicle dynamic sensors during GNSS outages," *J. Sensors*, vol. 2017, Jul. 2017, Art. no. 9802610.

[32] K. Takeyama, T. Machida, Y. Kojima, and N. Kubo, "Improvement of dead reckoning in urban areas through integration of low-cost multisensors," *IEEE Trans. Intell. Vehicles*, vol. 2, no. 4, pp. 278–287, Dec. 2017.

[33] F. Liu, Y. B. Sarvrood, and Y. Gao, "Implementation and analysis of tightly integrated INS/Stereo VO for land vehicle navigation," *J. Navigat.*, vol. 71, no. 1, pp. 83–99, Jan. 2018.

[34] U. Iqbal, A. F. Okou, and A. Noureldin, "An integrated reduced inertial sensor system—RISS/GPS for land vehicle," in *Proc. IEEE/ION Position, Location Navigat. Symp.*, May 2008, pp. 1014–1021.

[35] J. Georgy, A. Noureldin, M. J. Korenberg, and M. M. Bayoumi, "Low-cost three-dimensional navigation solution for RISS/GPS integration using mixture particle filter," *IEEE Trans. Veh. Technol.*, vol. 59, no. 2, pp. 599–615, Feb. 2010.

[36] M. Cossaboom, J. Georgy, T. Karamat, and A. Noureldin, "Augmented Kalman filter and map matching for 3D RISS/GPS integration for land vehicles," *Int. J. Navigat. Observ.*, vol. 2012, 2012, Art. no. 576807.

[37] M. M. Atia, T. Karamat, and A. Noureldin, "An enhanced 3D multi-sensor integrated navigation system for land-vehicles," *J. Navigat.*, vol. 67, no. 4, pp. 651–671, 2014.

[38] M. Ilyas, Y. Yang, Q. S. Qian, and R. Zhang, "Low-cost IMU/odometer/GPS integrated navigation aided with two antennae heading measurement for land vehicle application," in *Proc. 25th Chin. Control Decis. Conf. (CCDC)*, May 2013, pp. 4521–4526.

[39] H. Li, X. Xiao, B. Wang, and Z. Deng, "Nonholonomic constrained navigation algorithm for MIMU/odometer integration," in *Proc. 17th Int. IEEE Conf. Intell. Transp. Syst. (ITSC)*, Oct. 2014, pp. 2440–2445.

[40] J. Gao, K. Li, and Y. Chen, "Study on integration of FOG single-axis rotational INS and odometer for land vehicle," *IEEE Sensors J.*, vol. 18, no. 2, pp. 752–763, Jan. 2018.

[41] W. Jia, X. Xiao, and Z. Deng, "Self-calibration of INS/odometer integrated system via Kalman filter," in *Proc. IEEE 5th Int. Conf. Adv. Comput. Intell. (ICACI)*, Oct. 2012, pp. 224–228.

[42] W. Qingzhe, F. Mengyin, X. Xuan, and D. Zhihong, "Automatic calibration and in-motion alignment of an odometer-aided ins," in *Proc. 31st Chin. Control Conf. (CCC)*, Jul. 2012, pp. 2024–2028.

[43] Y. Wu, "Versatile land navigation using inertial sensors and odometry: Self-calibration, in-motion alignment and positioning," in *Proc. DGON Inertial Sensors Syst. (ISS)*, Sep. 2014, pp. 1–19.

[44] L. Zhu and W. Wang, "CDGPS-based calibration of odometer's scale factor with temperature for vehicle navigation system," in *Proc. Int. Conf. Optoelectron. Image Process. (ICOIP)*, vol. 1, Nov. 2010, pp. 317–320.

[45] A. Abosekeen, A. Noureldin, and M. J. Korenberg, "Utilizing the ACC-FMCW radar for land vehicles navigation," in *Proc. IEEE/ION Position, Location Navigat. Symp. (PLANS)*, Apr. 2018, pp. 124–132.

[46] P. Gao, K. Li, L. Wang, and Z. Liu, "A self-calibration method for accelerometer nonlinearity errors in triaxis rotational inertial navigation system," *IEEE Trans. Instrum. Meas.*, vol. 66, no. 2, pp. 243–253, Feb. 2017.

WOO JUNG PARK received the B.S. degree in mechanical and aerospace engineering and the M.S. degree in interdisciplinary program of bioengineering from Seoul National University, South Korea, in 2014 and 2016, respectively, where he is currently pursuing the Ph.D. degree with the Department of Mechanical and Aerospace Engineering. His current research interests include target tracking and land vehicle navigation.

JIN WOO SONG (M'96) received the B.S. and M.S. degrees in control and instrumentation engineering from Seoul National University, in 1995 and 1997, respectively, and the Ph.D. degree in electrical, electronic, and computer engineering from Seoul National University, in 2002. From 2003 to 2014, he was with Microinfinity Company, Ltd., as a CTO. Since 2014, he has been a Research Professor for BK21Plus Transformative Training Program for Creative Mechanical and Aerospace Engineers with the Department of Mechanical and Aerospace Engineering, Seoul National University, Seoul, South Korea. From 2016 to 2017, he was an Assistant Professor with the Department of Robotics Engineering, Hoseo University, Asan, South Korea. He is currently an Assistant Professor with the School of Intelligent Mechatronic Engineering, Sejong University, Seoul. His research interests include GPS/INS integration, robust and optimal control, MEMS inertial sensors and systems, indoor navigation, and robot localization.

CHANG HO KANG received the B.S. degree in mechanical and aerospace engineering from Sejong University, in 2009, and the Ph.D. degree from the Department of Mechanical and Aerospace Engineering, Seoul National University, in 2016. He held a postdoctoral position with the BK21+ Transformative Training Program for Creative Mechanical and Aerospace Engineers with Seoul National University, from 2016 to 2018. He is currently a Research Professor with the Research Institute of Engineering and Technology, Korea University. His research interests include global navigation satellite system (GNSS) receivers, digital signal processing, nonlinear filtering, and multi-target tracking.

JAE HONG LEE received the B.S. degree from the School of Mechanical and Electrical Control Engineering, Handong Global University, and the M.S. degree from the Department of Mechanical and Aerospace Engineering, Seoul National University, Seoul, South Korea, in 2017 and 2019, respectively, where he is currently pursuing the Ph.D. degree with the Department of Mechanical and Aerospace Engineering. His research interests are pedestrian dead reckoning, and inertial navigation systems.

MYUNG HWAN SEO received the B.S. and M.S. degrees in information and telecommunication engineering from Korea Aerospace University, South Korea, in 2008 and 2010, respectively. He is currently a Senior Research Engineer with Hyundai MNSOFT, Seoul, South Korea. His current research interests include dead reckoning and visual inertial odometry (VIO).

SANG YEON PARK received the B.S. degree in mechanical and geoinformatic engineering from Inha University, South Korea, in 2011. He is currently a Researcher with Hyundai MNSOFT, Seoul, South Korea. His current research interests include INS and visual inertial odometry (VIO).

JONG YUN YEO received the B.S. and M.S. degrees from the School of Electrical Engineering, Kookmin University, Seoul, South Korea, in 2010 and 2012, respectively. He is currently a Researcher with Hyundai MNSOFT, Seoul. His current research interests include INS and visual inertial odometry (VIO).

CHAN GOOK PARK received the B.S., M.S., and Ph.D. degrees in control and instrumentation engineering from Seoul National University, South Korea, in 1985, 1987, and 1993, respectively. He has worked with Prof. J. L. Speyer on peak seeking control for formation flight with the University of California (UCLA), Los Angeles, CA, USA, as a Postdoctoral Fellow, in 1998. From 1994 to 2003, he was with Kwangwoon University, Seoul, South Korea, as an Associate Professor. In 2003, he joined the faculty of the School of Mechanical and Aerospace Engineering, Seoul National University, South Korea, where he is currently a Professor. From 2009 to 2010, he was a Visiting Scholar with the Department of Aerospace Engineering, Georgia Institute of Technology, Atlanta, GA, USA. His current research topics include advanced filtering techniques, high precision INS, GPS/INS integration, MEMS-based pedestrian dead reckoning, and visual inertial navigation. He has served as the Chair of the IEEE AES Korea Chapter, until 2009.